

Groundstate fidelity phase diagram of the fully anisotropic two-leg spin- $\frac{1}{2}$ XXZ ladder

Sheng-Hao Li^{1,2}, Qian-Qian Shi^{1,3}, Murray T. Batchelor^{1,4} and Huan-Qiang Zhou¹

¹ Centre for Modern Physics and Department of Physics, Chongqing University, Chongqing 400044, The People's Republic of China

² Chongqing Vocational Institute of Engineering, Chongqing 402260, The People's Republic of China

³ College of Materials Science and Engineering and Centre for Modern Physics, Chongqing University, Chongqing 400044, The People's Republic of China

⁴ Mathematical Sciences Institute and Department of Theoretical Physics, Research School of Physics and Engineering, Australian National University, Canberra ACT 2601, Australia

Abstract. The fully anisotropic two-leg spin- $\frac{1}{2}$ XXZ ladder model is studied in terms of an algorithm based on the tensor network representation of quantum many-body states as an adaptation of projected entangled pair states to the geometry of translationally invariant infinite-size quantum spin ladders. The tensor network algorithm provides an effective method to generate the groundstate wave function, which allows computation of the groundstate fidelity per lattice site, a universal marker to detect phase transitions in quantum many-body systems. The groundstate fidelity is used in conjunction with local order and string order parameters to systematically map out the groundstate phase diagram of the ladder model. The phase diagram exhibits a rich diversity of quantum phases. These are the ferromagnetic, stripe ferromagnetic, rung singlet, rung triplet, Néel, stripe Néel and Haldane phases, along with the two XY phases $XY1$ and $XY2$.

PACS numbers: 74.20.-z, 02.70.-c, 71.10.Fd

Keywords: XXZ spin ladder, quantum phases, quantum fidelity, tensor networks

1. Introduction

Spin ladder systems have attracted considerable attention from both experimentalists and theoreticians alike [1, 2]. One of the most striking features of the simple spin- $\frac{1}{2}$ Heisenberg ladder is that the spin excitations are gapful (gapless) when the number of legs is even (odd) [3]. Spin ladder systems in general represent a particularly interesting class of quantum critical phenomena, exhibiting a rich variety of quantum phases [4, 5, 6, 7, 8]. Apart from a few cases [2], spin ladder systems are not exactly

solvable, therefore it is necessary to develop various techniques, both analytical and numerical, to investigate their physical properties [9, 10, 11, 12, 13, 14, 15, 16, 17, 18, 19].

An efficient tensor network (TN) algorithm has been developed which is tailored to translationally invariant infinite-size spin ladder systems [20]. The algorithm is based on an adaptation to the ladder geometry of projected entangled pair states [21], a representation of quantum many-body wave functions. The spin ladder TN algorithm has been successfully applied to a variety of models [20, 22], including the ferromagnetic frustrated two-leg ladder, the two-leg Heisenberg spin ladder with cyclic four-spin exchange and cross couplings, and the three-leg Heisenberg spin ladder with staggering dimerization. The algorithm is seen to be efficient compared to the density matrix renormalization group [12] and time evolving block decimation [23], at least as far as the memory cost is concerned.

The TN representation offers an efficient way to detect quantum phase transitions in many-body quantum systems [24, 25] using the groundstate fidelity per lattice site [26, 27, 29, 28, 30, 31] (for other work on the fidelity approach to quantum phase transitions, see also [32, 33, 34, 35]). We recall that fidelity, as a measure of quantum state distinguishability in quantum information science, describes the distance between two given quantum states. It offers a powerful means to investigate critical phenomena in quantum many-body lattice systems, as demonstrated in Refs. [26, 27, 29, 28, 30, 31]. For example, the groundstate fidelity per lattice site enables the characterization of drastic changes of the groundstate wave functions in the vicinity of a phase transition point. A systematic scheme to study critical phenomena in quantum many-body lattice systems has been outlined using this approach [36]. Once the groundstate phase diagram is mapped out by means of the groundstate fidelity per lattice site, the local order parameters can be derived from the reduced density matrices for a representative groundstate wave function in a symmetry-broken phase. Other phases without any long-range order can also be detected and further characterized by nontrivial order parameters such as string order and pseudo-order parameters.

In this paper we use the TN algorithm developed in Ref. [20] to study a two-leg ladder model with anisotropic spin- $\frac{1}{2}$ XXZ interactions along the legs and rungs of the ladder. A schematic phase diagram for this ladder model was mapped out previously using the sublattice entanglement of the groundstates [37]. A variant of this ladder model, with isotropic rung interactions, was shown to exhibit a rich phase diagram [9, 38]. We perform an extensive numerical analysis of the fully anisotropic model to map out the groundstate phase diagram by evaluating the groundstate fidelity per lattice site from the groundstate wave functions. The phase transition points and thus the phase boundaries are detected through identifying pinch points on the groundstate fidelity surfaces, which arise from the distinct changes of the groundstate wave functions in the vicinity of the critical points as the model parameters are varied across a transition point. This requires a scan of the entire parameter space. The phase diagram unveiled in this way is shown in Figure 1. Varying the XXZ anisotropy parameter Δ and the relative rung coupling strength J is seen to result in a rich diversity

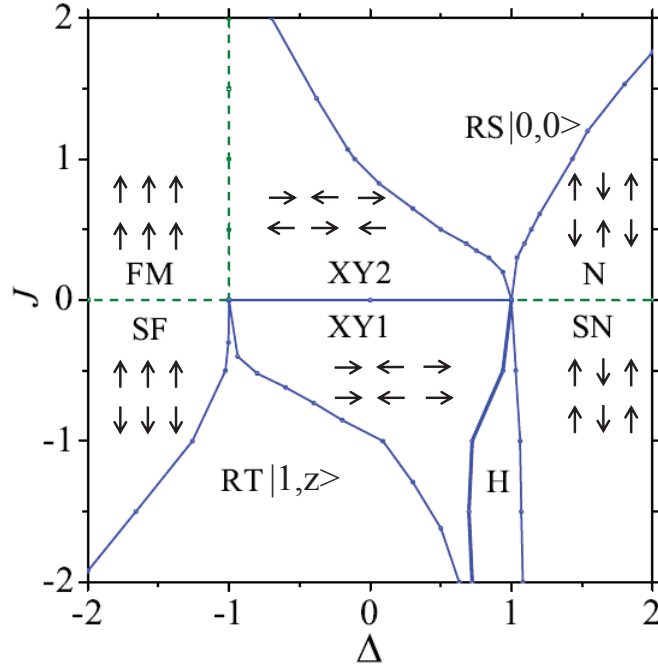


Figure 1. The groundstate phase diagram of the spin- $\frac{1}{2}$ XXZ two-leg ladder model (1) in the Δ - J plane obtained from the groundstate fidelity and tensor network approach. The various lines denote the phase boundaries between the nine different phases. These are the ferromagnetic (FM), stripe ferromagnetic (SF), rung singlet (RS), rung triplet (RT), Néel (N), stripe Néel (SN), Haldane (H) and XY (XY_1 and XY_2) phases. Dashed lines denote a first-order phase transition and solid lines denote a continuous phase transition.

of phases – ferromagnetic (FM), stripe ferromagnetic (SF), rung singlet (RS), rung triplet (RT), Néel (N), stripe Néel (SN), Haldane (H) and two XY phases (XY_1 and XY_2). In particular, when $|\Delta| > 1$ the resulting Ising-type anisotropy breaks any continuous spin symmetry, in contrast to the XY -type regime for $|\Delta| < 1$. The XY -type phases without any long-range order are characterized in terms of string order parameters. In the symmetry-broken phases local order parameters are constructed from reduced density matrices for a representative groundstate wave function. In the XY -type regime varying the rung coupling J induces magnetic phases beyond standard ferromagnetism, for example, the rung-singlet and Haldane phases. For this model, we detect an additional rung-triplet phase as a result of the inherent competition between singlet formation and magnetic ordering.

The layout of the paper is as follows. The fully anisotropic spin- $\frac{1}{2}$ XXZ two-leg ladder model is described in Section 2, with the results using the TN algorithm presented in detail in Section 3. Concluding remarks, along with a discussion of previous results for this model, are given in Section 4.

2. The model

The fully anisotropic spin- $\frac{1}{2}$ XXZ two-leg ladder system can be considered as a pair of infinitely long spin chains coupled via rung interactions. All spin interactions are of the spin- $\frac{1}{2}$ XXZ Heisenberg type. The Hamiltonian is defined by

$$H = H_{\text{leg}} + H_{\text{rung}}, \quad (1)$$

where

$$H_{\text{leg}} = \sum_i \sum_{\alpha=1,2} (S_{\alpha,i}^x S_{\alpha,i+1}^x + S_{\alpha,i}^y S_{\alpha,i+1}^y + \Delta S_{\alpha,i}^z S_{\alpha,i+1}^z), \quad (2)$$

$$H_{\text{rung}} = J \sum_i (S_{1,i}^x S_{2,i}^x + S_{1,i}^y S_{2,i}^y + \Delta S_{1,i}^z S_{2,i}^z). \quad (3)$$

Here $S_{\alpha,i}^{\beta}$ ($\beta = x, y, z$) is the spin- $\frac{1}{2}$ operator acting at site i on the α -th leg, J is the rung coupling between the two spins on a rung, and Δ is the XXZ anisotropy parameter. Our aim is to map out the groundstate phase diagram of this model in the Δ - J plane.

In the FM phase, the ladder system orders ferromagnetically in both the leg and rung directions, whereas in the SF phase it orders ferromagnetically in the leg direction and antiferromagnetically in the rung direction. In contrast, in the N phase, the system orders antiferromagnetically in both the leg and rung directions, whereas in the SN phase it orders antiferromagnetically in the leg direction and ferromagnetically in the rung direction. Notice that in the FM, SF, N, and SN phases $\langle S_{\alpha,i}^x \rangle = \langle S_{\alpha,i}^y \rangle = 0$ and $\langle S_{\alpha,i}^z \rangle \neq 0$.

The critical XY phases belong to the universality class of the Tomonaga-Luttinger liquid [39], which is known to exhibit a power-law decay of the spin-spin correlations with gapless excitations. The possibility for the existence of two different XY phases in a ladder system was pointed out in a slightly different model [17]. According to the Marshall-Lieb-Mattis theorem [40], the $XY1$ phase is in the $J < 0$ region and the $XY2$ phase is in the $J > 0$ region of the parameter space. Long-range order does not exist in the XY phases in the thermodynamic limit. Nevertheless, there is a practical way to characterize the XY phases in the context of the TN representation of the groundstate wave functions, which is achieved by defining a pseudo-order parameter arising from the finiteness of the bond dimension χ [31]. This offers a convenient means to numerically determine the phase boundaries between the XY phase and other phases. For the $XY1$ and $XY2$ phases, $\langle S_{\alpha,i}^z \rangle = 0$ and $\langle S_{\alpha,i}^x \rangle^2 + \langle S_{\alpha,i}^y \rangle^2 \neq 0$.

The two-spin states on a rung are written as

$$|0,0\rangle = \frac{1}{\sqrt{2}}(|\uparrow_1\downarrow_2\rangle - |\downarrow_1\uparrow_2\rangle),$$

$$|1,x\rangle = \frac{1}{\sqrt{2}}(|\downarrow_1\downarrow_2\rangle - |\uparrow_1\uparrow_2\rangle),$$

$$|1,y\rangle = \frac{i}{\sqrt{2}}(|\downarrow_1\downarrow_2\rangle + |\uparrow_1\uparrow_2\rangle),$$

$$|1,z\rangle = \frac{1}{\sqrt{2}}(|\uparrow_1\downarrow_2\rangle + |\downarrow_1\uparrow_2\rangle).$$

Here the subscripts 1 and 2 label the different spins on the same rung (see, e.g., Ref. [41]). The first state is the singlet and the remaining three states constitute the triplet. As can readily be seen from the Hamiltonian (1), the groundstate of the system in the strong coupling limit $J \rightarrow \pm\infty$ corresponds to the RS ($|0,0\rangle$) and RT ($|1,z\rangle$) phases, respectively. It should be noted that the RS phase, the RT phase and the H phase lack long-range order in the conventional Landau-Ginzburg-Wilson sense. However, each are characterized by a suitably modified string order parameter [42]. For the RS, RT and H phases $\langle S_{\alpha,i}^\beta \rangle = 0$.

3. Results

To map out the groundstate phase diagram, we first consider the regions $J > 0$ and $J < 0$, with the anisotropy Δ as a control parameter. We then fix Δ and vary the rung coupling J . Illustrative examples are given in detail below for the values $J = \pm 1$. In our approach, apart from order parameters, which we also make use of, the groundstate fidelity per lattice site is used as an important tool to detect quantum phase transitions. For two different groundstates $|\psi(x)\rangle$ and $|\psi(x')\rangle$ in a quantum system corresponding to different values x and x' of a control parameter, the fidelity $F(x, x') = |\langle\psi(x)|\psi(x')\rangle|$ is defined as a measure of the overlap between the two states. For large but finite size N , the fidelity F scales as d^N , with d interpreted as the ground state fidelity per site $d = \lim_{N \rightarrow \infty} F_N^{1/N}$. As a well-defined property even in the thermodynamic limit, the groundstate fidelity per lattice site d enjoys some properties inherited from the fidelity F , namely: (i) symmetry under interchange, $d(x, x') = d(x', x)$; (ii) normalization, $d(x, x) = 1$; (iii) range $0 \leq d(x, x') \leq 1$.

In previous studies the fidelity per lattice site d was demonstrated to be a useful detector for different types of quantum phase transition via its singularity structure [27, 28, 26, 29, 30, 31]. In this approach, a pinch point in the $d(x, x')$ surface occurs at a quantum phase transition, i.e., at each phase transition point x_c , a pinch point (x_c, x_c) occurs on the surface of fidelity per lattice site $d(x, x')$ at the crossing of two singular lines $x = x_c$ and $x' = x_c$. In these studies the groundstate wavefunctions are determined using TN algorithms [21, 43]. The combined groundstate fidelity and TN approach has been tailored to include ladder systems [20].

A key point in the investigation of the two-leg quantum spin ladders via the TN approach is that the computational cost scales as χ^6 , where χ is the bond dimension for each of the four necessary four-index tensors. These tensors need to be updated simultaneously, with the updating procedure closely related to the infinite PEPS [44] and translationally invariant MPS [45] algorithms. A summary of the TN approach for quantum spin ladders is given in Appendix A. For the spin- $\frac{1}{2}$ isotropic XXX two-leg ladder it was demonstrated earlier that the TN approach could accurately determine the groundstate wave function, with bond dimension $\chi = 6$ outperforming the DMRG results [20]. Of necessity for the calculation of the order parameters, the reduced density matrix ρ can be computed directly from the TN representation of the groundstate wave

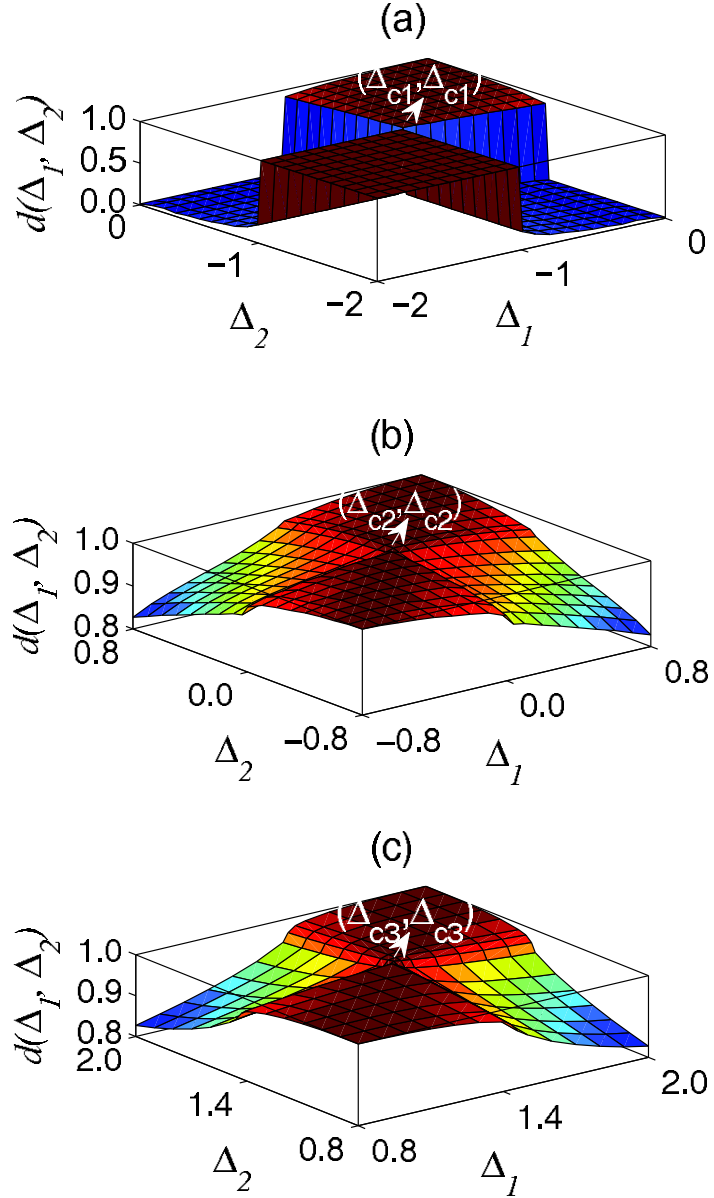


Figure 2. The groundstate fidelity surface $d(\Delta_1, \Delta_2)$ for the spin- $\frac{1}{2}$ XXZ two-leg ladder model (1) for rung coupling $J = 1$ and varying anisotropy Δ calculated with bond dimension $\chi = 6$. Three pinch points are identified at $(\Delta_{c1}, \Delta_{c1})$, $(\Delta_{c2}, \Delta_{c2})$ and $(\Delta_{c3}, \Delta_{c3})$ on the global fidelity surface, indicating three phase transition points, located at (a) $\Delta_{c1} = -1.00$, (b) $\Delta_{c2} = 0.00$ and (c) $\Delta_{c3} = 1.43$.

functions [20]. The reduced density matrix displays different nonzero-entry structures in different phases.

3.1. $J = 1, -2 \leq \Delta \leq 2$

Fixing the rung coupling to the value $J = 1$ and varying the anisotropy parameter Δ from -2 to 2 , we are able to determine the phase boundaries between the FM phase,

the $XY2$ phase, the RS phase and the Néel phase. The groundstate fidelity per site, $d(\Delta_1, \Delta_2)$, is shown in Figure 2 as a function of Δ_1 and Δ_2 , calculated with bond dimension $\chi = 6$. Here the range of the plots is restricted to highlight the fidelity surface and, in particular, the pinch points. The results in Figure 2(a) and Figure 2(c) differ very little for a larger bond dimension χ , indicating that the computational results are almost saturated for bond dimension $\chi = 6$. However, the pinch point in Figure 2(b) shifts noticeably when χ increases from $\chi = 6$ to $\chi = 12$, as Figure 3 shows. Three pinch points are identified at $(\Delta_{c1}, \Delta_{c1})$, $(\Delta_{c2}, \Delta_{c2})$ and $(\Delta_{c3}, \Delta_{c3})$ on the fidelity surfaces, indicating that there are three phase transition points. These are located at (i) $\Delta_{c1} = -1.00$, (ii) $\Delta_{c2} = 0.00$ and (iii) $\Delta_{c3} = 1.43$. In this way we are able to identify four different phases, separated by three transition points. It remains to characterize these phases in terms of local or nonlocal order parameters.

In the FM phase, the one-site reduced density matrix yields the local order parameter,

$$O_{\text{FM}} = \frac{1}{2} |\langle (S_{1,i}^z + S_{2,i}^z) + (S_{1,i+1}^z + S_{2,i+1}^z) \rangle|. \quad (4)$$

Our numerical results indicate that the ladder system is in the FM phase for $\Delta < -1.00$ (see Figure 3(a)).

In the Néel phase, we similarly consider the local order parameter

$$O_{\text{N}} = \frac{1}{2} |\langle (S_{1,i}^z - S_{2,i}^z) - (S_{1,i+1}^z - S_{2,i+1}^z) \rangle|. \quad (5)$$

In the Néel phase, the Néel order O_{N} exhibits a long-range order. The evaluation of the order parameter indicates that the ladder system is in the Néel phase for $\Delta > 1.43$ (see Figure 3(a)).

In the RS phase, the groundstate wave function may be approximated by the product of local rung singlets. As usual, two distinct string order parameters, O_{odd} and O_{even} , may be used to characterize the RS phase. For two-leg ladder models these are defined by

$$O_{\text{odd/even}} = - \lim_{|i-j| \rightarrow \infty} \left\langle S_{\text{o/e},i}^z \exp \left[i\pi \sum_{l=i+1}^{j-1} S_{\text{o/e},l}^z \right] S_{\text{o/e},j}^z \right\rangle, \quad (6)$$

where $S_{\text{o},i}^z \equiv S_{1,i}^z + S_{2,i}^z$ and $S_{\text{e},i}^z \equiv S_{1,i}^z + S_{2,i+1}^z$. The odd and even string order parameters are actually mutually exclusive in the RS, RT and H phases. Our results for O_{odd} and O_{even} indicate that the RS phase persists in the region $\Delta_{c2} < \Delta < \Delta_{c3}$ with $J = 1$ (see Figure 3(a)).

In the XY phases, the TN algorithm automatically leads to infinite degenerate groundstates, arising from pseudo spontaneous symmetry breaking of the continuous $U(1)$ symmetry, due to the finiteness of the bond dimension χ . This allows the introduction of a pseudo-order parameter that must scale to zero, in order to keep consistency with the Mermin-Wagner theorem. As suggested in Refs. [31] and [41], the pseudo-order parameters in the $XY1$ and $XY2$ phases may be defined as

$$O_1 = \sqrt{\langle S_{1,i}^x + S_{2,i}^x \rangle^2 + \langle S_{1,i}^y + S_{2,i}^y \rangle^2}, \quad (7)$$

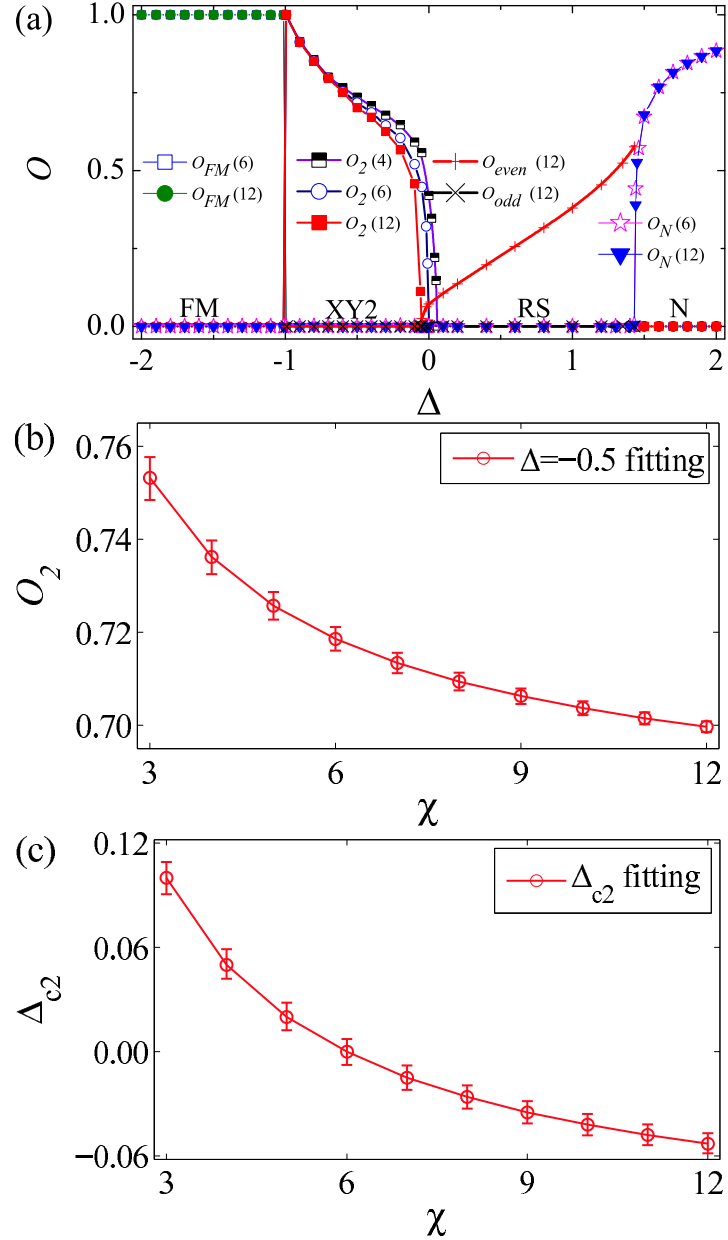


Figure 3. (a) The local order parameter $O_{FM}(\chi)$ in the FM phase, the pseudo-order parameter $O_2(\chi)$ in the XY2 phase, the local order parameter $O_N(\chi)$ in the Néel phase and the string order parameters $O_{odd}(\chi)$ and $O_{even}(\chi)$ in the RS phase as a function of the anisotropy Δ , with $J = 1$. Three phase transition points, Δ_{c1} , Δ_{c2} and Δ_{c3} , are distinguished by the behavior of the order parameters. The phase transition points $\Delta_{c1} = -1.00$ and $\Delta_{c3} = 1.43$ are saturated for bond dimension $\chi = 6$, whereas Δ_{c2} shifts with increasing χ . (b) The scaling of the pseudo-order parameter $O_2(\chi)$ for $\Delta = -0.5$ (see text). (c) The “pseudo-critical” point estimates $\Delta_{c2}(\chi)$ obtained from the pseudo-order parameter $O_2(\chi)$ and their fitting function (see text).

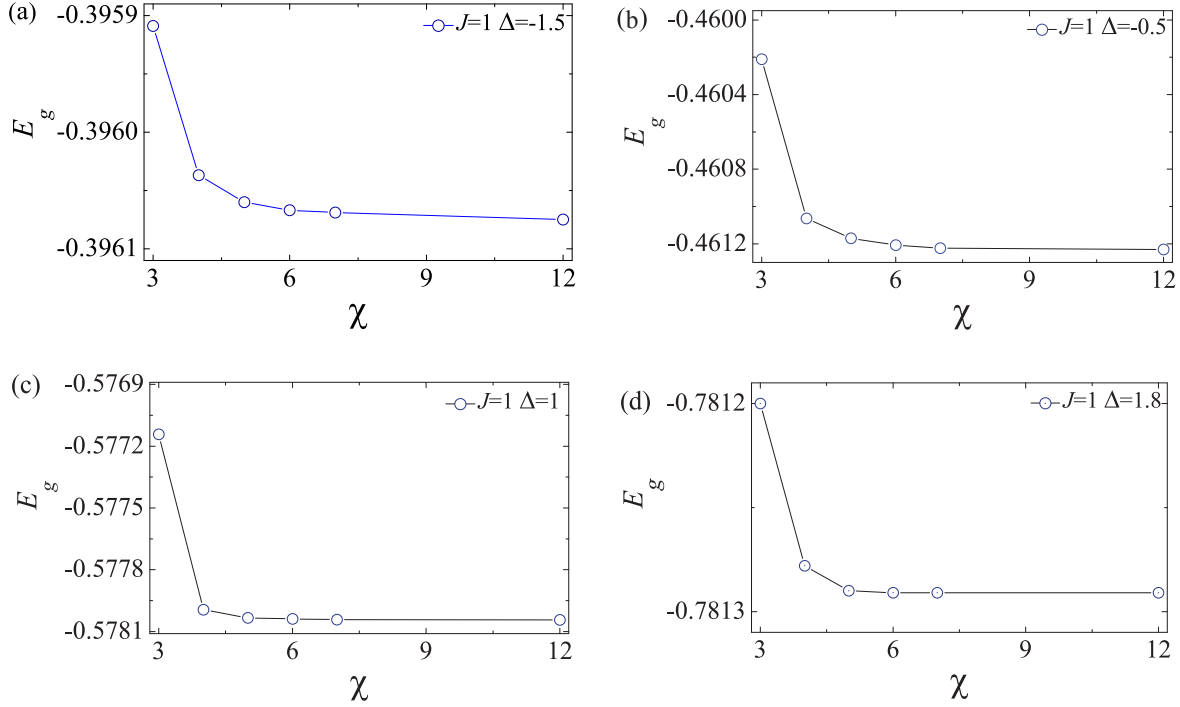


Figure 4. Convergence of the groundstate energy E_g with increasing bond dimension $\chi = 3, 4, 5, 6, 7, 12$ in different phases with rung coupling $J = 1$ and anisotropy parameter values (a) $\Delta = -1.5$ (FM phase) (b) $\Delta = -0.5$ (XY2 phase) (c) $\Delta = 1.0$ (RS phase) (d) $\Delta = 1.8$ (N phase).

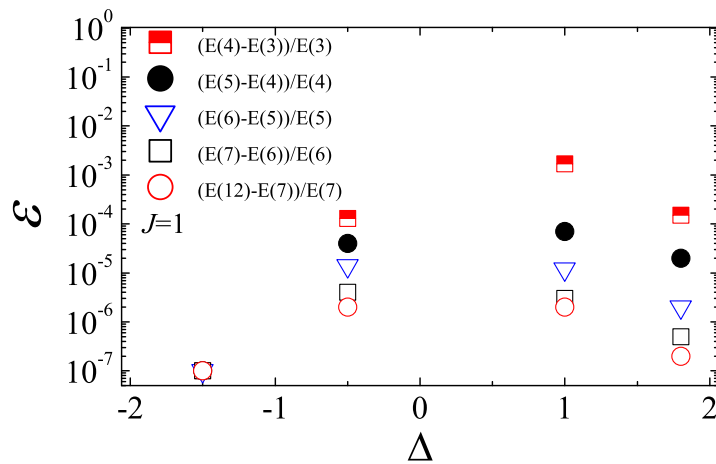


Figure 5. Relative error ε in the estimates of the groundstate energy as a function of Δ at $J = 1$ for increasing bond dimension χ . The relative errors are defined by $\varepsilon = (E(\chi_{n+1}) - E(\chi_n))/E(\chi_n)$ where $E(\chi_n)$ is the groundstate energy estimate for given bond dimension χ_n .

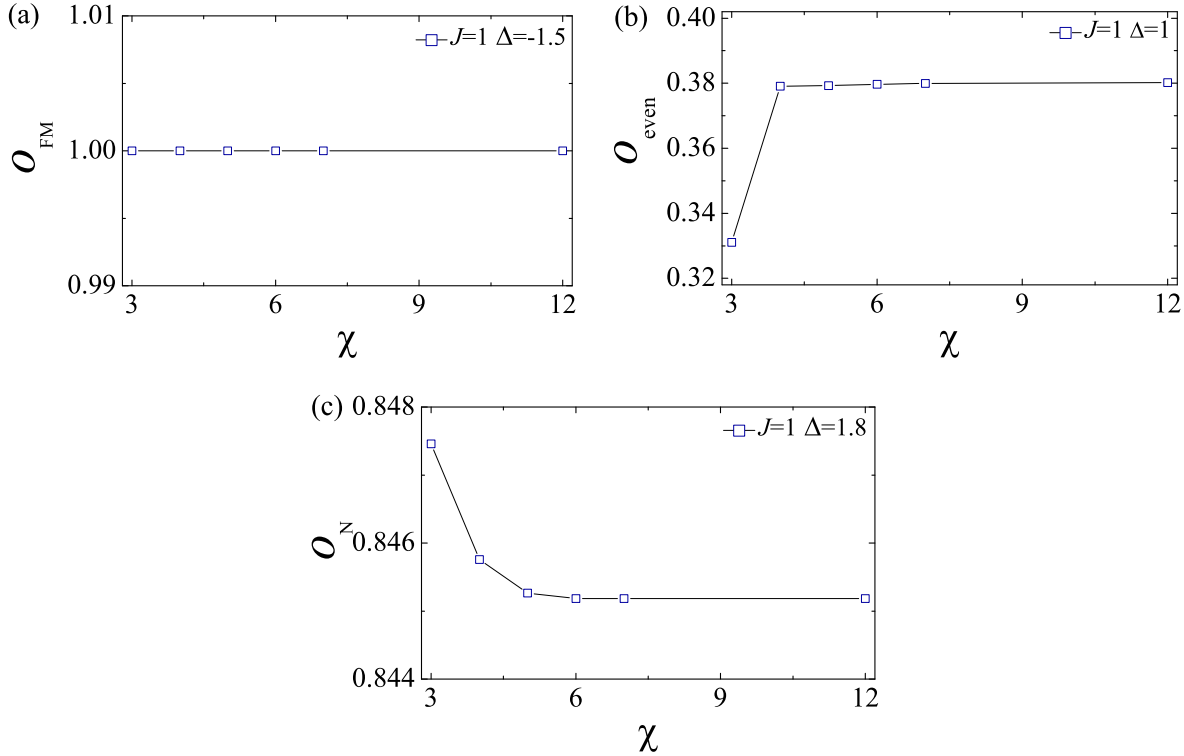


Figure 6. Convergence of order parameters with increasing bond dimension $\chi = 3, 4, 5, 6, 7, 12$ in different phases for $J = 1$. (a) local order parameter O_{FM} for $\Delta = -1.5$ (FM phase). (b) string order parameter O_{even} for $\Delta = 1.0$ (RS phase). (c) local order parameter O_N for $\Delta = 1.8$ (N phase).

and

$$O_2 = \sqrt{\langle S_{1,i}^x - S_{2,i}^x \rangle^2 + \langle S_{1,i}^y - S_{2,i}^y \rangle^2}. \quad (8)$$

The pseudo-order parameter O_2 in the $XY2$ phase is plotted as a function of the anisotropy Δ for different values of the bond dimension χ in Figure 3(a). This order parameter O_2 is also plotted as a function of χ for $\Delta = -0.5$ in Figure 3(b). It is clearly seen that O_2 decreases as χ increases. Here the pseudo-order parameter scales to zero according to $O_2(\chi) = a_1 \chi^{-b_1} (1 + c_1 \chi^{-1})$, with $a_1 = 0.697(3)$, $b_1 = 0.007(1)$ and $c_1 = 0.26(1)$. Such scaling was adopted in previous studies of pseudo-order parameters [31, 41] and ensures that they vanish for infinite bond dimension as expected.

The estimates of the “pseudo-critical” values $\Delta_{c2}(\chi)$ at which the pseudo-order parameter $O_2(\chi)$ becomes zero are shown in Figure 3(c). These points are extrapolated with respect to the bond dimension χ , with an extrapolation function $\Delta(\chi) = a_2 + b_2 \chi^{-c_2}$. The results imply the fitting constants $a_2 = -0.110(2)$, $b_2 = 0.585(7)$ and $c_2 = 0.93(2)$. In the limit $\chi \rightarrow \infty$ we have $\Delta(\infty) = a_2$, which is the estimate for the critical point Δ_{c2} between the $XY2$ and RS phases. The term “pseudo-critical” point is used because such estimates are obtained using the pseudo-order parameters. Nevertheless they yield estimates for real critical points.

The existence of the FM phase, the $XY2$ phase, the Néel phase and the RS phase is numerically confirmed in this way, as seen from Figure 3. Specifically, the three phase transition points occur at the values $\Delta_{c1} = -1.00$, $\Delta_{c2} \simeq -0.11$ and $\Delta_{c3} = 1.43$. If the anisotropy coupling Δ is tuned as a control parameter, the ladder system undergoes a first-order phase transition at Δ_{c1} , with continuous phase transitions at Δ_{c2} and Δ_{c3} . The different nature of the first-order transition at Δ_{c1} can be seen clearly in the fidelity surface in Figure 2(a), compared to the continuous transitions in Figure 2(b) and Figure 2(c). In general, for continuous phase transitions, the fidelity surface shows continuous behaviour near critical points, while discontinuous phase transitions show discontinuous behaviour.

In the limit $J \rightarrow \infty$ the $XY2$ phase vanishes. In addition for general $J > 0$ the line $\Delta = -1$ is the phase boundary between the FM phase $\Delta < -1$ and the $XY2$ phase $\Delta > -1$. We have also confirmed that $\Delta \approx J$ is the phase boundary between the RS phase and the Néel phase, when $\Delta \rightarrow \infty$ and $J \rightarrow \infty$. There are thus three phases when $J \rightarrow \infty$: the FM phase, the RS phase and the Néel phase.

Concerning the accuracy of our results, estimates of the groundstate energy per site with increasing bond dimension are shown in Figure 4. The estimates are seen to converge rapidly, as quantified in Figure 5. We find that almost all of the relative errors reach to order 10^{-5} . This indicates the reliability of the algorithm for generating accurate groundstate wave functions for spin ladders, given a preset error tolerance. The corresponding convergence of the order parameter estimates is shown in Figure 6. As is well understood, states in gapless phases, such as the $XY1$ and $XY2$ phases, are more difficult to compute than states in phases with a large gap, such as the FM, N and SF phases, which converge much faster, yielding the same accuracy with a smaller bond dimension. Phases with a small gap, such as the H phase, are also more difficult to compute. In general this slower convergence in gapless (critical) versus gapped phases is a feature of numerical entanglement based approaches, such as TN methods [43]. This is because the overall strategy of the TN method is more efficient for gapped systems. By design, the finite bond dimension already induces a gap in the system. From the perspective of entanglement in quantum critical phenomena [46], gapped systems obey an area law, which can be well described using relatively small bond dimensions. On the other hand, for gapless systems, the entanglement diverges as the gap vanishes, requiring larger, in principle infinite, bond dimensions. Alternatively, for the same size bond dimension, more iteration steps are necessary for convergence in gapless compared to gapped systems. Our algorithm is seen to work sufficiently well in the phases under consideration. However, the critical $XY1$ and $XY2$ phases require additional extrapolation to infinite-size bond dimension.

3.2. $J = -1, -2 \leq \Delta \leq 2$

In similar fashion, we determine the phase boundaries between the SF, RT ($|1, z\rangle$), $XY1$, H and SN phases. The groundstate fidelity per lattice site $d(\Delta_1, \Delta_2)$ is shown

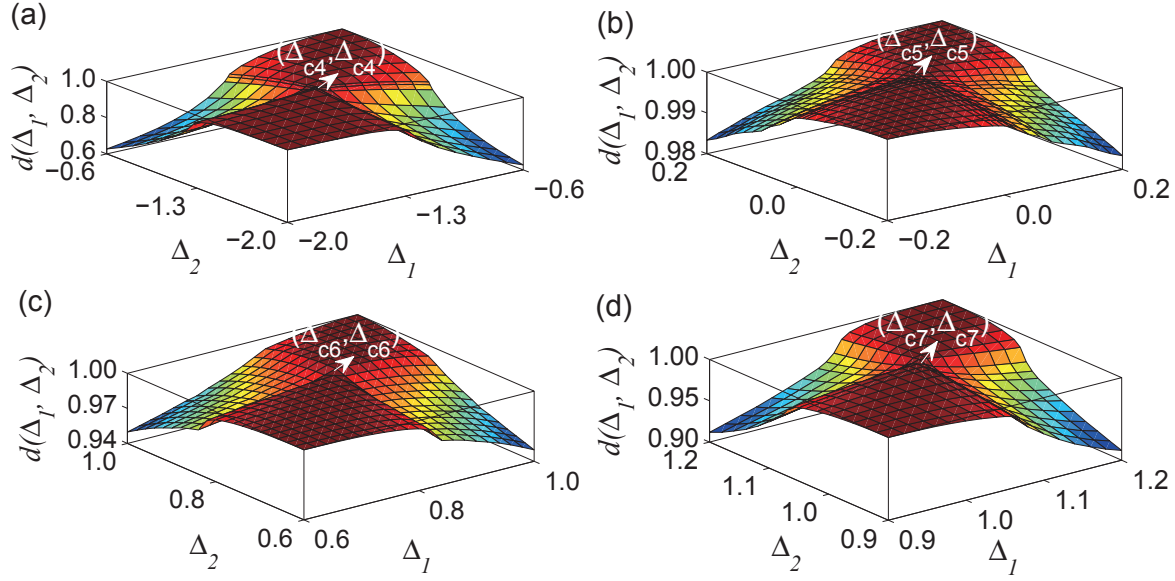


Figure 7. The groundstate fidelity surface $d(\Delta_1, \Delta_2)$ for the spin- $\frac{1}{2}$ XXZ two-leg ladder model (1) for rung coupling $J = -1$ and varying anisotropy Δ calculated with bond dimension $\chi = 6$. Four pinch points are identified at $(\Delta_{c4}, \Delta_{c4})$, $(\Delta_{c5}, \Delta_{c5})$, $(\Delta_{c6}, \Delta_{c6})$ and $(\Delta_{c7}, \Delta_{c7})$ on the global fidelity surface, indicating four phase transition points, located at (a) $\Delta_{c4} = -1.26$, (b) $\Delta_{c5} = 0.00$, (c) $\Delta_{c6} = 0.84$, and (d) $\Delta_{c7} = 1.06$.

as a function of Δ_1 and Δ_2 in Figure 7 with bond dimension $\chi = 6$. In this region four pinch points, $(\Delta_{c4}, \Delta_{c4})$, $(\Delta_{c5}, \Delta_{c5})$, $(\Delta_{c6}, \Delta_{c6})$ and $(\Delta_{c7}, \Delta_{c7})$, are identified on the fidelity surfaces, corresponding to the continuous phase transition points $\Delta_{c4} = -1.26$, $\Delta_{c5} = 0.00$, $\Delta_{c6} = 0.84$ and $\Delta_{c7} = 1.06$. These points separate five different phases, which we now proceed to characterize in terms of the order parameters.

In the SF phase, the one-site reduced density matrix yields the local order parameter

$$O_{\text{SF}} = \frac{1}{2} |\langle (S_{1,i}^z - S_{2,i}^z) + (S_{1,i+1}^z - S_{2,i+1}^z) \rangle|. \quad (9)$$

Our results show that the ladder system exhibits a long-range order in the SF phase for $\Delta < -1.26$ (see Figure 8(a)).

In the SN phase, we are similarly able to consider the local order parameter

$$O_{\text{SN}} = \frac{1}{2} |\langle (S_{1,i}^z + S_{2,i}^z) - (S_{1,i+1}^z + S_{2,i+1}^z) \rangle|. \quad (10)$$

In this phase the ladder system exhibits a long-range order for $\Delta > 1.06$ (see Figure 8(a)).

In the H phase, the even string order parameter O_{even} vanishes, but the odd string order parameter is nonzero. Conversely, in the RT ($|1, z\rangle$) phase, $O_{\text{odd}} = 0$ and the even string order parameter is nonzero (see Figure 8(a)).

In the XY1 phase, the pseudo-order parameter O_1 as a function of the anisotropy Δ for different bond dimension χ is shown in Figure 8(a). The pseudo-order parameter is plotted as a function of χ for $\Delta = 0.5$ in Figure 8(b). Here we have performed an

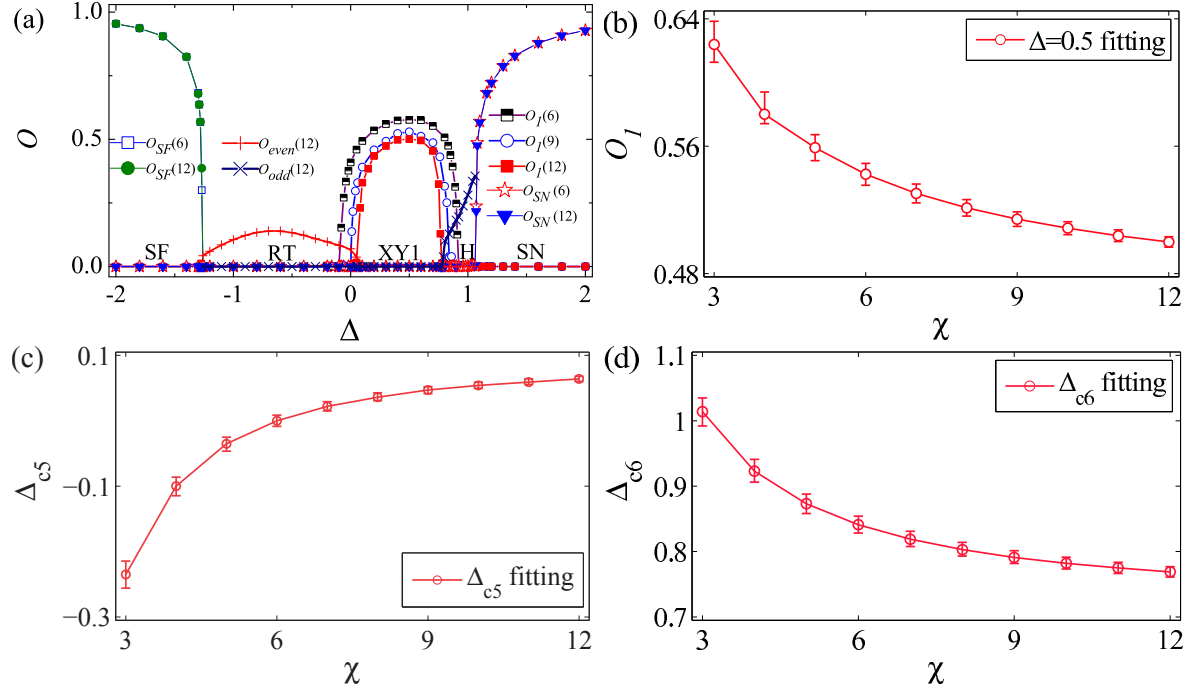


Figure 8. (a) The local order parameters O_{SF} in the SF phase and O_{SN} in the SN phase, the pseudo-order parameter O_1 in the XY1 phase and the string order parameters O_{odd} and O_{even} in the Haldane and RT ($|1, z\rangle$) phases as a function of the anisotropy Δ , with $J = -1$. Two phase transition points are identified at $\Delta_{c4} = -1.26$ and $\Delta_{c7} = 1.06$ for $\chi = 6$, with no significant shift observed for increasing χ . The other two phase transition estimates, Δ_{c5} and Δ_{c6} , shift with increasing χ . (b) The pseudo-order parameter estimates $O_1(\chi)$ for $\Delta = 0.5$ in the XY1 phase (see text). (c) The “pseudo-critical” point estimates $\Delta_{c5}(\chi)$ obtained from the pseudo-order parameter $O_1(\chi)$ and its fitting function (see text). (d) The “pseudo-critical” point estimates $\Delta_{c6}(\chi)$ obtained from the pseudo-order parameter $O_1(\chi)$ and its fitting function (see text).

extrapolation with respect to χ , with the fitting function $O_1(\chi) = a_3 \chi^{-b_3} (1 + c_3 \chi^{-1})$, where $a_3 = 0.467(7)$, $b_3 = 0.006(4)$ and $c_3 = 1.04(5)$. This is again consistent with previous studies of pseudo-order parameters. The estimates of the “pseudo-critical” points $\Delta_{c5}(\chi)$ and $\Delta_{c6}(\chi)$ on either side of the XY1 phase are shown in Figure 8(c) and Figure 8(d). Here we employ the extrapolation functions $\Delta_{c5}(\chi) = a_4 + b_4 \chi^{-c_4}$ and $\Delta_{c6}(\chi) = a_5 + b_5 \chi^{-c_5}$. Numerical fitting yields $a_4 = 0.088(2)$, $b_4 = -2.54(7)$ and $c_4 = 1.88(2)$ for the phase transition between the RT ($|1, z\rangle$) and XY1 phases with the values $a_5 = 0.718(2)$, $b_5 = 1.18(4)$ and $c_5 = 1.26(3)$ for the phase transition between the XY1 and H phases. In the limit $\chi \rightarrow \infty$ this yields the two critical point estimates Δ_{c5} and Δ_{c6} .

It follows that we have been able to compute the order parameters O_{SF} and O_{SN} in the SF and SN phases, the pseudo-order parameter O_1 in the XY1 phase, the string order parameter O_{even} in the RT ($|1, z\rangle$) phase, and the string order parameter O_{odd} in the H phase. The results are shown in Figure 8. With the anisotropy Δ as control

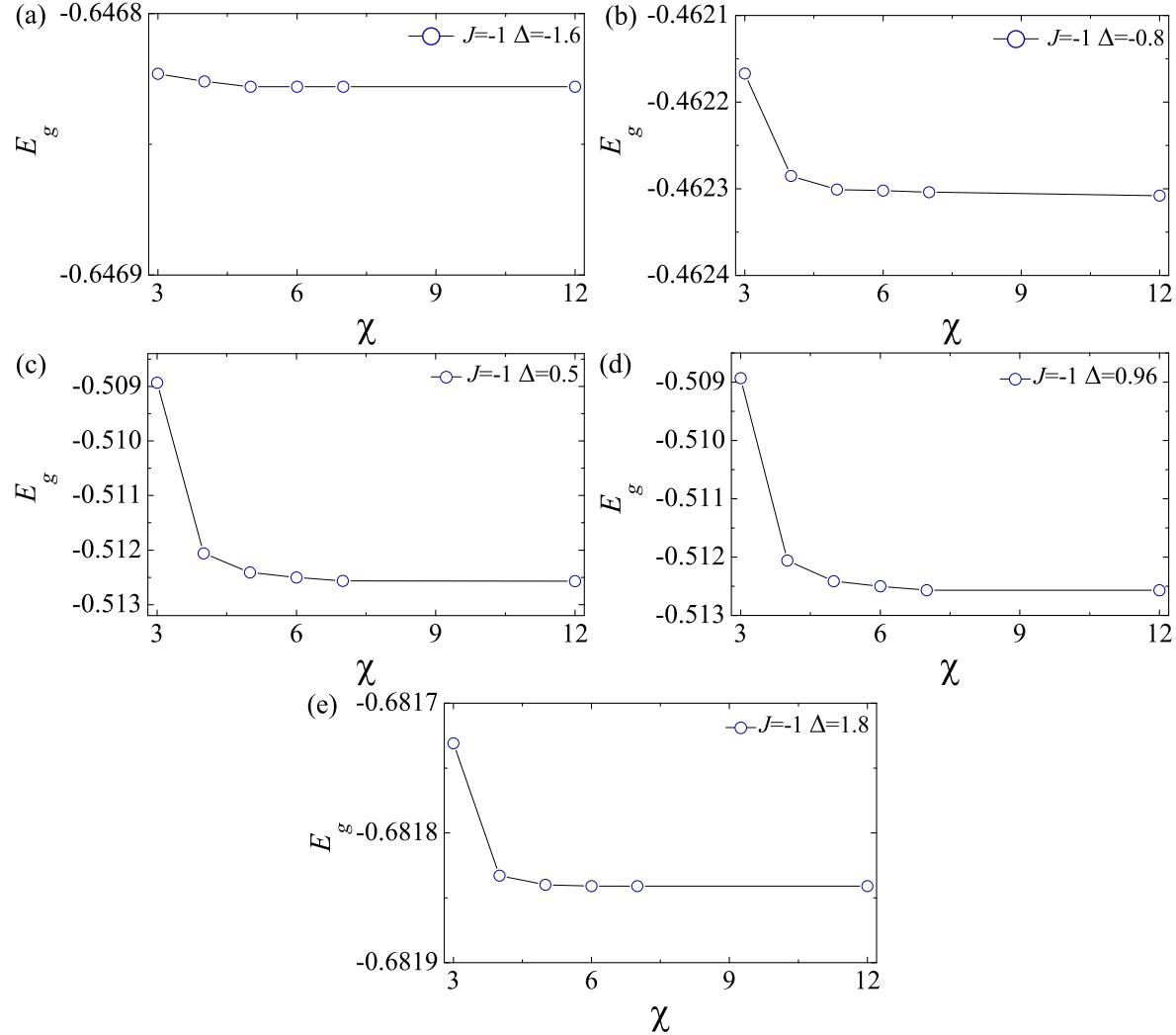


Figure 9. Convergence of the groundstate energy E_g with increasing bond dimension $\chi = 3, 4, 5, 6, 7, 12$ in different phases with rung coupling $J = -1$ and anisotropy parameter values (a) $\Delta = -1.6$ (SF phase) (b) $\Delta = -0.8$ (RT phase) (c) $\Delta = 0.5$ (XY1 phase) (d) $\Delta = 0.96$ (Haldane phase) (e) $\Delta = 1.8$ (SN phase).

parameter, the ladder system undergoes four continuous phase transitions at the values Δ_{c4} , Δ_{c5} , Δ_{c6} and Δ_{c7} .

In the limit $J \rightarrow -\infty$ the XY1 phase and the H phase vanish. We note that the phase boundary between the SF phase and the RT ($|1, z\rangle$) phase is located roughly near the line $\Delta \approx J$ in the limits $\Delta \rightarrow -\infty$ and $J \rightarrow -\infty$, while the phase boundary between the RT ($|1, z\rangle$) and SN phases is located roughly near the line $\Delta \sim 1$ as $J \rightarrow -\infty$. As a result there are three phases for the ladder system in the limit $J \rightarrow -\infty$, i.e., the SF, RT ($|1, z\rangle$) and SN phases.

The accuracy of the results is similar to that for $J > 0$, with estimates of the groundstate energy per site with increasing bond dimension shown in Figure 9. The estimates also converge rapidly, as quantified in Figure 10. The corresponding

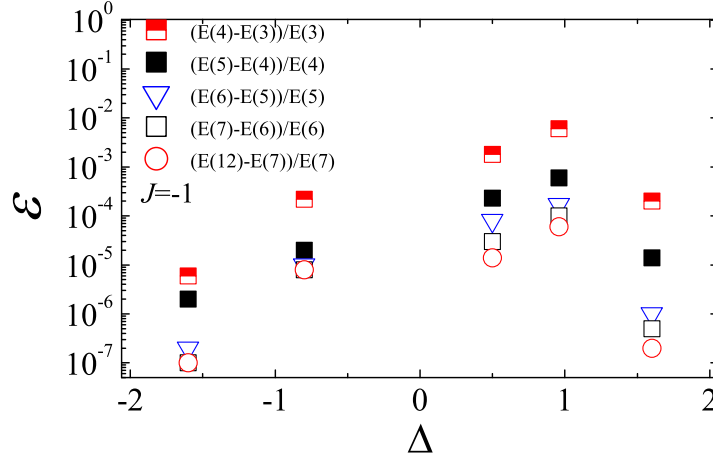


Figure 10. Relative error ε in the estimates of the groundstate energy as a function of Δ at $J = -1$ for increasing bond dimension χ . The relative errors are defined by $\varepsilon = (E(\chi_{n+1}) - E(\chi_n))/E(\chi_n)$ where $E(\chi_n)$ is the groundstate energy estimate for given bond dimension χ_n .

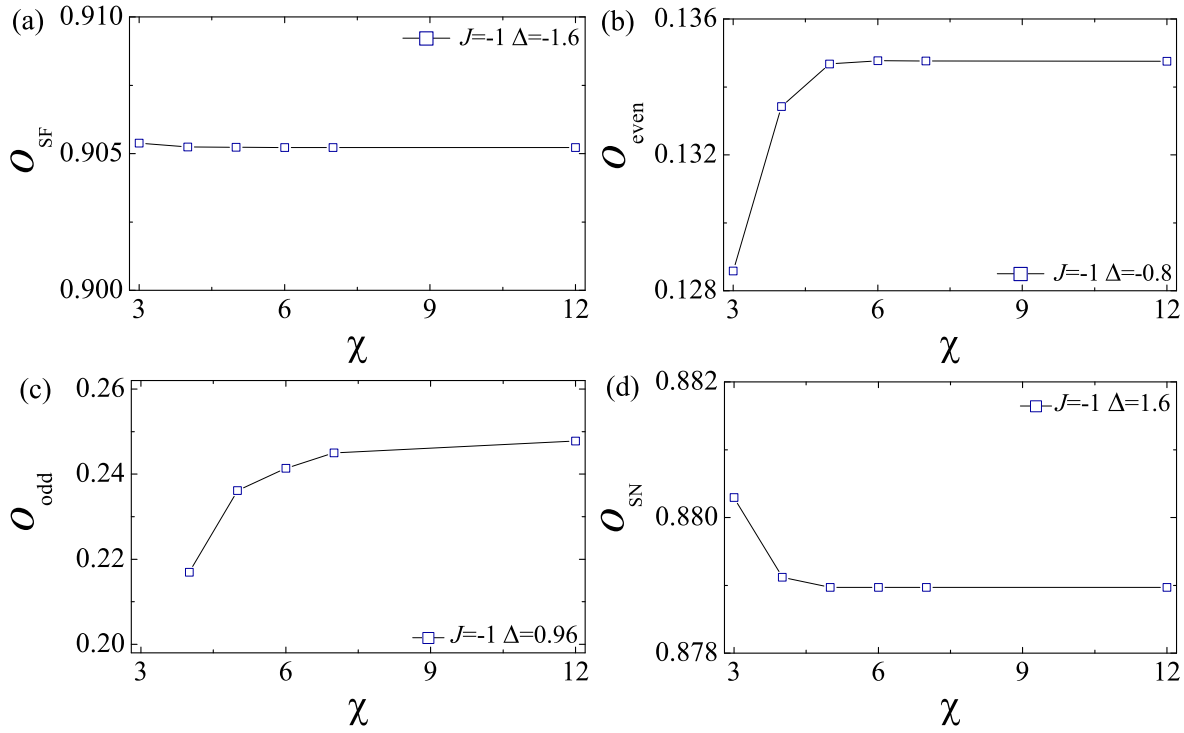


Figure 11. Convergence of order parameters with increasing bond dimension $\chi = 3, 4, 5, 6, 7, 12$ in different phases for $J = -1$. (a) local order parameter O_{SF} for $\Delta = -1.6$ (SF phase). (b) string order parameter O_{even} for $\Delta = 0.8$ (RT phase). (c) string order parameter O_{odd} for $\Delta = 0.96$ (H phase). (d) local order parameter O_{SN} for $\Delta = 1.6$ (SN phase).

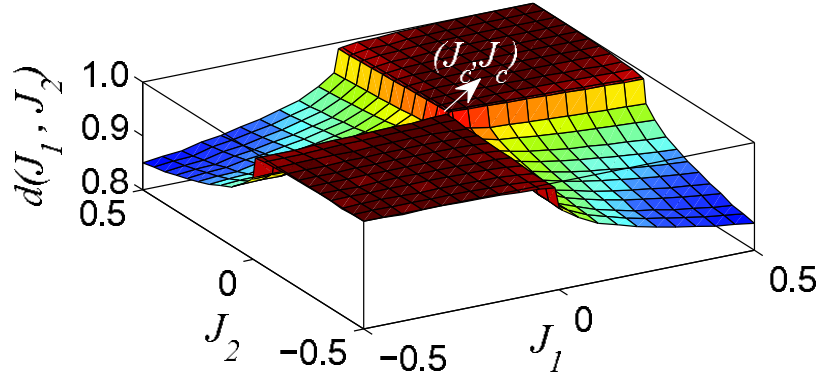


Figure 12. The groundstate fidelity surface $d(J_1, J_2)$ for the spin- $\frac{1}{2}$ XXZ two-leg ladder model (1) for anisotropy parameter $\Delta = 0$ and varying rung coupling with bond dimension $\chi = 6$. The pinch point occurring at $(J_c = 0.00, J_c = 0.00)$ indicates a continuous phase transition point.

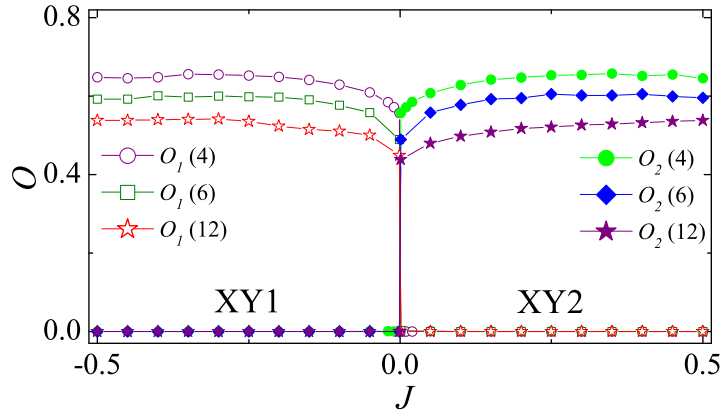


Figure 13. The pseudo-order parameter $O_1(\chi)$ in the $XY1$ phase and the pseudo-order parameter $O_2(\chi)$ in the $XY2$ phase as a function of the rung coupling J . The bond dimension values are $\chi = 4, 6, 12$.

convergence of the order parameter estimates is shown in Figure 11.

3.3. $\Delta = 0, -0.5 \leq J \leq 0.5$

We now turn to look more closely at the XY phase, which as we have seen, splits into the two different $XY1$ and $XY2$ phases identified by the local pseudo-order parameters O_1 and O_2 obtained from the groundstate fidelity per lattice site. As we shall see, for $-1 \leq \Delta \leq 1$, the phase boundary between the $XY1$ and $XY2$ phases is the line $J = 0$. Here we fix the anisotropy coupling $\Delta = 0$ and take J as control parameter in the range $-0.5 \leq J \leq 0.5$ to sweep across this boundary.

Figure 12 shows a plot of the groundstate fidelity per site $d(J_1, J_2)$ with bond dimension $\chi = 6$. In this case there is a clear indication of a continuous phase transition point at $J = 0.00$, as a pinch point occurs at this value with bond dimension $\chi = 6$.

Figure 13 shows a plot of the pseudo-order parameter O_1 in the $XY1$ phase and the pseudo-order parameter O_2 in the $XY2$ phase as a function of J . As already remarked, a feature of the pseudo-order parameters is that they vanish as the bond dimension χ increases.

4. Conclusion

We have systematically investigated the groundstate phase diagram of the infinite fully anisotropic spin- $\frac{1}{2}$ XXZ two-leg ladder model (1). This has been achieved by exploiting a TN algorithm tailored to the geometry of quantum spin ladder systems [20], allowing efficient evaluation of the groundstate fidelity per lattice site from the TN representation of the groundstate wave functions for the infinite-size quantum spin ladder. Illustrative results have been presented in Sec. III along the lines $J = \pm 1$ with varying Δ and the line $\Delta = 0$ with varying J . Our computational results using the groundstate fidelity per lattice site are consistent with results obtained from the construction of local, and where appropriate, nonlocal, order parameters in the different phases.

The full phase diagram, as obtained by this approach, is shown in Figure 1. This phase diagram, featuring nine distinct quantum phases, points to the rich diversity of physics in the fully anisotropic spin- $\frac{1}{2}$ XXZ two-leg ladder model. The precise nature of the phase diagram is a significant extension on the previously obtained schematic phase diagram for this model, which was mapped out by identifying ridges and valleys in contour plots of the rescaled block entanglement entropy corresponding to possible phase boundaries [37]. With that approach, which was aimed at demonstrating the usefulness of sublattice entanglement entropy as a means of exploring quantum phase transitions across a range of different spin systems, the nature and number of the different phases of the ladder model were not discussed in detail. The phase diagram of the fully anisotropic spin- $\frac{1}{2}$ XXZ two-leg ladder model also differs in significant aspects compared to the phase diagram of the spin- $\frac{1}{2}$ XXZ two-leg ladder model with isotropic rung interactions, the precise nature of which has been the subject of debate [9, 38]. With isotropic rung interactions, the model also exhibits FM, SF, RS, N, SN, H, $XY1$ and $XY2$ phases. However, for the fully anisotropic model considered here, there is an additional rung-triplet (RT($|1, z\rangle$)) phase, with the $XY1$ and $XY2$ phases extending over the whole $-1 \leq \Delta \leq 1$ region in the vicinity of $J \approx 0$. Moreover, the extent of the Haldane (H) phase is seen to be significantly diminished for fully anisotropic interactions. In general the difference between both the number of quantum phases and the phase diagrams of the two models highlights the key role played by anisotropies in the competition between singlet formation and magnetic ordering in quantum spin systems.

Acknowledgments

We thank Sam Young Cho, Bing-Quan Hu and Fabian Essler for helpful discussions at various stages of this work. The work is supported by Chongqing Research Program of Basic Research and Frontier Technology (Grant No. cstc2016jcyjA0480), National Natural Science Foundation of China (Grant No. 11575037, 11374379, 11174375) and by the Science and Technology Research Program of Chongqing Municipal Education Commission (Grant No. KJ1732433).

Appendix A. Tensor network representation for the spin- $\frac{1}{2}$ two-leg ladder

In this Appendix we summarise the relevant details of the TN representation for spin ladders [20]. The hamiltonian of the two-leg ladder model (1) under consideration is of the general form $H = \sum_i h_i$, with h_i acting on the i th plaquette between sites i and $i+1$ along a leg. The index i runs over all possible plaquettes with $i \in \{-\infty, \dots, +\infty\}$. It is sufficient to assume that the TN representation for the wave function is translational invariant under shifts by two lattice sites along the legs. The groundstate wave function for an infinite length ladder can be described by the four different four-index tensors $A_{\ell rd}^s$, $B_{\ell rd}^s$, $C_{\ell ru}^s$ and $D_{\ell ru}^s$. The tensor $A_{\ell rd}^s$ is depicted in Figure A1(i), with $s = 1, 2$ for spin- $\frac{1}{2}$ and with $\ell, r, u, d = 1, \dots, \chi$, the four inner bond indices, where χ is the bond dimension. A TN representation for the groundstate wave function is shown in Figure A1(ii) with one of the two equivalent choices shown for the plaquette (unit cell).

A gradient-directed random walk method is applied to compute the groundstates. The double tensors $a_{\tilde{\ell}\tilde{r}\tilde{d}}$, $b_{\tilde{\ell}\tilde{r}\tilde{d}}$, $c_{\tilde{\ell}\tilde{r}\tilde{u}}$ and $d_{\tilde{\ell}\tilde{r}\tilde{u}}$ are introduced, with $\tilde{\ell} = (\ell, \ell')$, $\tilde{r} = (r, r')$, $\tilde{u} = (u, u')$ and $\tilde{d} = (d, d')$. They are formed from the tensors $A_{\ell rd}^s$, $B_{\ell rd}^s$, $C_{\ell ru}^s$ and $D_{\ell ru}^s$, and their complex conjugates, as depicted in Figure A1(i) for the double tensor a . With these double tensors, the TN for the norm of a wave function is shown in Figure A1(iii). The two different but equivalent choices for the transfer matrix T are made from the plaquettes $abdc$ and $bacd$. In the above, the notation $\tilde{\ell} = (\ell, \ell')$ corresponds to the two independent indices ℓ and ℓ' , with $\tilde{\ell} = 1, 2, \dots, \chi^2$. Similarly for \tilde{r} , \tilde{u} and \tilde{d} .

For a randomly chosen initial state $|\psi_0\rangle$, the energy per plaquette e is

$$e = \frac{\langle \psi_0 | (h_{ABDC} + h_{BACD}) | \psi_0 \rangle}{2 \langle \psi_0 | \psi_0 \rangle}. \quad (\text{A.1})$$

The groundstate energy per plaquette also admits a TN representation as shown in Figure A1(v) and (vi) for plaquette ABDC, which absorbs the operator h acting on a plaquette for an infinite-size spin ladder. For each choice of plaquette, the dominant left and right eigenvectors of the transfer matrix T constitute the environment tensors, visualised in Figure A1(iv) and (vi) for plaquette ABDC. In this way the energy per plaquette e_{ABDC} is obtained. The same procedure may be used to compute the energy per plaquette e_{BACD} for an operator acting on the i th plaquette BACD.

To update the TN representation, the energy gradient is computed with respect to

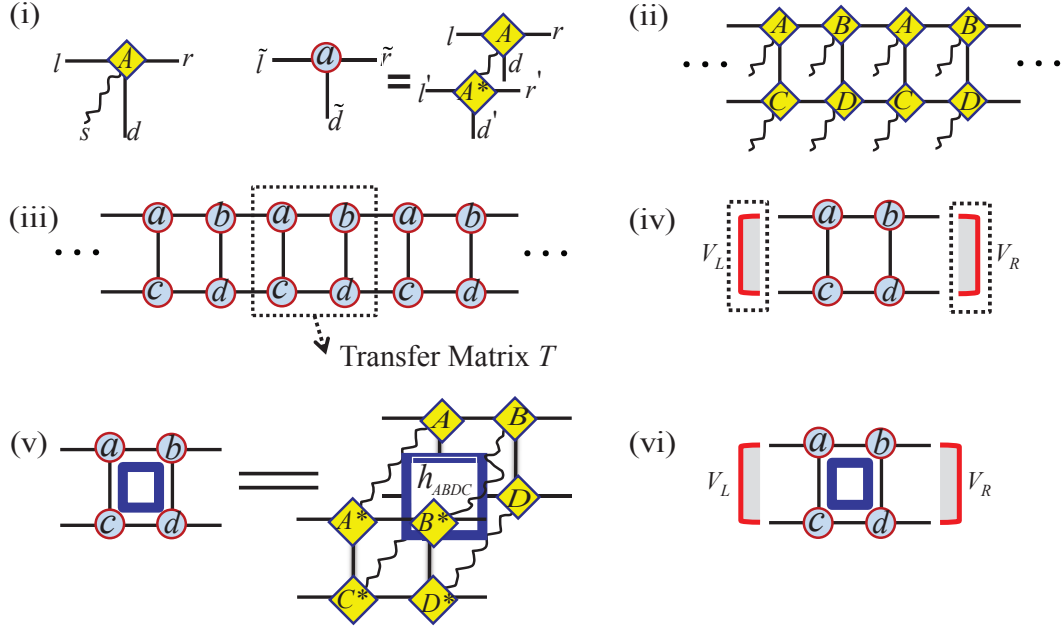


Figure A1. (i) Four-index tensor A_{\ellrd}^s used in the TN representation for the groundstate wave function for the infinite-size two-leg spin ladder. Also shown is the double tensor $a_{\tilde{\ell}\tilde{r}\tilde{d}}$ formed from the tensor A_{\ellrd}^s and its complex conjugate $(A^*)_{\ell'r'd'}^s$, with $\tilde{\ell} = (\ell, \ell')$, $\tilde{r} = (r, r')$ and $\tilde{d} = (d, d')$. (ii) Pictorial representation for a TN state $|\psi\rangle$ with leg and rung bonds, which are used to absorb an operator acting on the i th plaquette. (iii) TN representation for the norm of a groundstate wavefunction in the infinite ladder. Also shown is the transfer matrix T , which is constructed from the four double tensors $a_{\tilde{\ell}\tilde{r}\tilde{d}}$, $b_{\tilde{\ell}\tilde{r}\tilde{d}}$, $c_{\tilde{\ell}\tilde{r}\tilde{u}}$ and $d_{\tilde{\ell}\tilde{r}\tilde{u}}$, with $\tilde{\ell}$, \tilde{r} and \tilde{d} defined as above and $\tilde{u} = (u, u')$. (iv) The dominant left and right eigenvectors V_L and V_R of the transfer matrix T . (v) A unit cell with hamiltonian density h_{ABDC} acting on the plaquette ABDC. (vi) The groundstate energy per unit cell is computed from the eigenvectors V_L , V_R and the tensors A_{\ellrd}^s , B_{\ellrd}^s , C_{\ellru}^s and D_{\ellru}^s .

the tensor A_{\ellrd}^s , with

$$\frac{\partial e}{\partial A_{\ellrd}^s} = \frac{\partial \langle \psi_0 | H | \psi_0 \rangle / \partial A_{\ellrd}^s}{\langle \psi_0 | \psi_0 \rangle} - E_g \frac{\partial \langle \psi_0 | \psi_0 \rangle / \partial A_{\ellrd}^s}{\langle \psi_0 | \psi_0 \rangle}. \quad (\text{A.2})$$

The contributions to the energy gradient come from three parts (for a given choice of plaquette on which the hamiltonian acts), as shown in Figure A2. To obtain the energy gradient it is necessary to sum the contributions from both plaquettes $abdc$ and $bacd$. The tensor A_{\ellrd}^s is then updated according to

$$A_{\ellrd}^s = A_{\ellrd}^s - \delta \frac{\partial E_g / \partial A_{\ellrd}^s}{\max_{(\ell, r, d)} |\partial E_g / \partial A_{\ellrd}^s|}, \quad (\text{A.3})$$

where δ denotes the update step size. In this procedure the tensors A_{\ellrd}^s , B_{\ellrd}^s , C_{\ellru}^s and D_{\ellru}^s are updated simultaneously. Repeating this procedure until the groundstate energy per plaquette converges leads to the groundstate wave function as approximated in the TN representation.

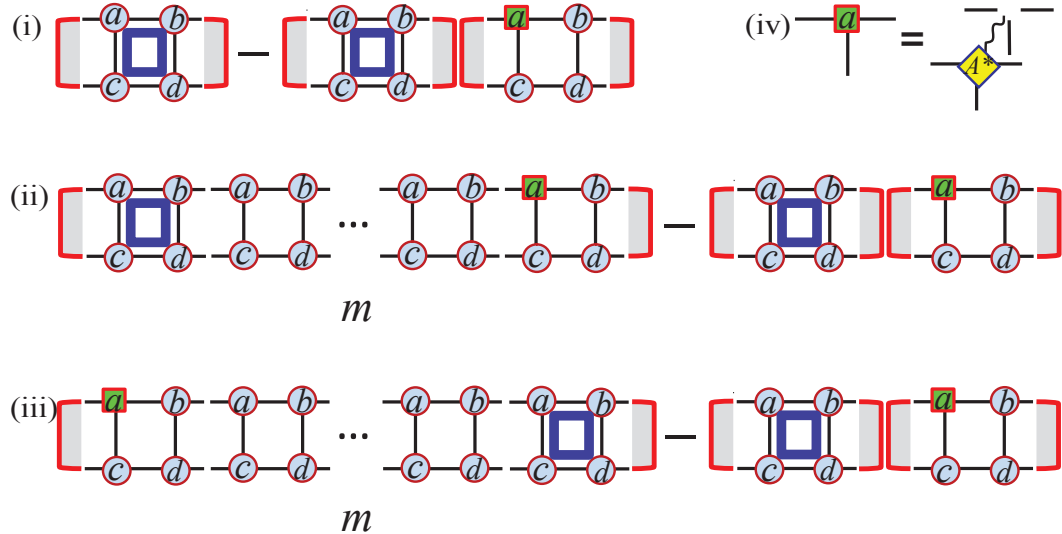


Figure A2. The contribution to the energy gradient (A.2) for the infinite-size spin ladder consists of three parts: (i), (ii) and (iii) depending on the location of the hole cell with tensor A_{lrd}^s removed. In the latter two cases, there are m cells between the hole and hamiltonian cell, where $m \in (0, 1, 2, 3, \dots)$. The hole cell is visualised in (iv), with the tensor A_{lrd}^s removed. Note that only the contribution from the plaquette $abdc$, as labeled here, is shown. There is also a similar contribution from the plaquette $bacd$.

References

- [1] Dagotto E and Rice T M 1996 Surprises on the way from one- to two-dimensional quantum magnets: The ladder materials *Science* **271** 618
Dagotto E 1999 Experiments on ladders reveal a complex interplay between a spin-gapped normal state and superconductivity *Rep. Prog. Phys.* **62** 1525
- [2] Batchelor M T, Guan X-W, Oelkers N and Tsuboi Z 2007 Integrable models and quantum spin ladders: comparison between theory and experiment for the strong coupling ladder compounds *Adv. Phys.* **56** 465
- [3] White S R, Noack R M and Scalapino D J 1994 Resonating valence-bond theory of coupled Heisenberg-chains *Phys. Rev. Lett.* **73** 886
- [4] Shelton D G, Nersesyan A A and Tsvelik A M 1996 Antiferromagnetic spin ladders: Crossover between spin $S = \frac{1}{2}$ and $S = 1$ chains *Phys. Rev. B* **53** 8521
- [5] Nersesyan A A and Tsvelik A M 1997 One-dimensional spin-liquid without magnon excitations *Phys. Rev. Lett.* **78** 3939
- [6] Fouet J-B, Mila F, Clarke D, Youk H, Tchernyshyov O, Fendley P and Noack R M 2006 Condensation of magnons and spinons in a frustrated ladder *Phys. Rev. B* **73** 214405
- [7] Meyer J S and Matveev K A 2009 Wigner crystal physics in quantum wires *J. Phys.: Condens. Matter* **21** 023203
- [8] Sheng D N, Motrunich O I, Trebst S, Gull E and Fisher M P A 2008 Strong coupling phases of frustrated bosons on a two-leg ladder with ring exchange *Phys. Rev. B* **78** 054520
- [9] Strong S P and Millis A J 1992 Competition between singlet formation and magnetic ordering in one-dimensional spin systems *Phys. Rev. Lett.* **69** 2419
Strong S P and Millis A J 1994 Competition between singlet formation and magnetic ordering in one-dimensional spin systems *Phys. Rev. B* **50** 9911

- [10] Watanabe H, Nomura K and Takada S 1993 $S = \frac{1}{2}$ quantum Heisenberg ladder and $S = 1$ Haldane phase *J. Phys. Soc. Jpn.* **62** 2845
- [11] Narushima T, Nakamura T and Takada S 1995 Numerical study on the ground-state phase-diagram of the $S = \frac{1}{2}$ XXZ ladder model *J. Phys. Soc. Jpn.* **64** 4322
- [12] White S R 1992 Density matrix formulation for quantum renormalization groups *Phys. Rev. Lett.* **69** 2863
White S R 1993 Density matrix algorithm for quantum renormalization groups *Phys. Rev. B* **48** 10345
- [13] Ueda M, Nagata T, Akimitsu J, Takahashi H, Môri N and Kinoshita K 1996 Superconductivity in the ladder material $Sr_{0.4}Ca_{13.6}Cu_{24}O_{41.84}$ *J. Phys. Soc. Jpn.* **65** 2764
- [14] Kolezhuk A K and Mikeska H-J 1996 Phase transitions in the Heisenberg spin ladder with ferromagnetic legs *Phys. Rev. B* **53** R8848
- [15] Kopina K, Tinus A M C and de Jonge W J M 1982 Magnetic behavior of the ferromagnetic quantum chain systems $(C_6H_{11}NH_3)CuCl_3$ (CHAC) and $(C_6H_{11}NH_3)CuBr_3$ (CHAB) *Phys. Rev. B* **25** 4685
- [16] Kopina K, Tinus A M C and de Jonge W J M 1984 Evidence for solitons in a quantum ($S = \frac{1}{2}$) XY system *Phys. Rev. B* **29** 2868R
- [17] Vekua T, Japaridze G I and Mikeska H-J 2003 Phase diagrams of spin ladders with ferromagnetic legs *Phys. Rev. B* **67** 064419
- [18] Legeza Ö and Sólyom J 1997 Stability of the Haldane phase in anisotropic magnetic ladders *Phys. Rev. B* **56** 14449
- [19] Lecheminant P and Orignac E 2002 Magnetization and dimerization profiles of the cut two-leg spin ladder *Phys. Rev. B* **65** 174406
- [20] Li S-H, Shi Q-Q, Su Y-H, Liu J-H, Dai Y-W and Zhou H-Q 2012 Tensor network states and ground-state fidelity for quantum spin ladders *Phys. Rev. B* **86** 064401
- [21] Verstraete F and Cirac J I 2004 Renormalization algorithms for quantum many-body systems in two and higher dimensions, arXiv:cond-mat/0407066
Cirac J I and Verstraete F 2009 Renormalization and tensor product states in spin chains and lattices *J. Phys. A* **42** 504004
- [22] Chen X-H, Cho S Y, Batchelor M T and Zhou H-Q 2016 The antiferromagnetic cross-coupled spin ladder: quantum fidelity and tensor networks approach *J. Kor. Phys. Soc.* **68** 1114
- [23] Vidal G 2007 Classical simulation of infinite-size quantum lattice systems in one spatial dimension *Phys. Rev. Lett.* **98** 070201
- [24] Sachdev S 1999 *Quantum Phase Transitions* (Cambridge: Cambridge University Press)
- [25] Wen X-G 2004 *Quantum Field Theory of Many-Body Systems* (Oxford: Oxford University Press)
- [26] Zhou H-Q and Barjaktarević J P 2008 Fidelity and quantum phase transitions *J. Phys. A* **41** 412001
- [27] Zhou H-Q, Zhao J-H and Li B 2008 Fidelity approach to quantum phase transitions: finite-size scaling for the quantum Ising model in a transverse field *J. Phys. A* **41** 492002
- [28] Zhou H-Q 2007 Renormalization group flows and quantum phase transitions: fidelity versus entanglement, arXiv:0704.2945
- [29] Zhou H-Q, Orús R and Vidal G 2008 Ground state fidelity from tensor network representations *Phys. Rev. Lett.* **100** 080601
- [30] Zhao J-H, Wang H-L, Li B and Zhou H-Q 2010 Spontaneous symmetry breaking and bifurcations in ground-state fidelity for quantum lattice systems *Phys. Rev. E* **82** 061127
- [31] Wang H-L, Zhao J-H, Li B and Zhou H-Q 2011 Kosterlitz-Thouless phase transition and ground state fidelity: a novel perspective from matrix product states *J. Stat. Mech.* L10001
- [32] Zanardi P and Paunković N 2006 Ground state overlap and quantum phase transitions *Phys. Rev. E* **74** 031123
- [33] Zanardi P, Cozzini M and Giorda P 2007 Ground state fidelity and quantum phase transitions in free Fermi systems *J. Stat. Mech.* L02002

Oelkers N and Links J 2007 Ground-state properties of the attractive one-dimensional Bose-Hubbard model *Phys. Rev. B* **75** 115119

Cozzini M, Ionicioiu R and Zanardi P 2007 Quantum fidelity and quantum phase transitions in matrix product states *Phys. Rev. B* **76** 104420

Campos Venuti L and Zanardi P 2007 Quantum critical scaling of the geometric tensors *Phys. Rev. Lett.* **99** 095701

Liu T, Zhang Y-Y, Chen Q-H and Wang K-L 2009 Large- N scaling behavior of the ground-state energy, fidelity, and the order parameter in the Dicke model *Phys. Rev. A* **80** 023810

[34] Gu S-J, Kwok H-M, Ning W-Q and Lin H-Q 2008 Fidelity susceptibility, scaling, and universality in quantum critical phenomena *Phys. Rev. B* **77** 245109

Yang M-F 2007 Ground-state fidelity in one-dimensional gapless models *Phys. Rev. B* **76** 180403(R)

Tzeng Y-C and Yang M-F 2008 Scaling properties of fidelity in the spin-1 anisotropic model *Phys. Rev. A* **77** 012311

Fjærstad J O 2008 Ground state fidelity of Luttinger liquids: a wavefunctional approach *J. Stat. Mech.* P07011

Sirker J 2010 Finite-temperature fidelity susceptibility for one-dimensional quantum systems *Phys. Rev. Lett.* **105** 117203

[35] Rams M M and Damski B 2011 Quantum fidelity in the thermodynamic limit *Phys. Rev. Lett.* **106** 055701

[36] Zhou H-Q 2008 Deriving local order parameters from tensor network representations, arXiv:0803.0585

[37] Chen Y, Zanardi P, Wang Z D and Zhang F C 2006 Sublattice entanglement and quantum phase transitions in antiferromagnetic spin chains *New J. Phys.* **8** 97

[38] Hijii K, Kitazawa A and Nomura K 2005 Phase diagram of $S = \frac{1}{2}$ two-leg XXZ spin-ladder systems *Phys. Rev. B* **72** 014449

[39] Tomonaga S 1950 Remarks on Bloch's method of sound waves applied to many-fermion problems *Prog. Theor. Phys.* **5** 544

Luttinger J M 1963 An exactly soluble model of a many-fermion system *J. Math. Phys.* **4** 1154

Mattis D C and Lieb E H 1965 Exact solution of a many-fermion system and its associated boson field *J. Math. Phys.* **6**, 304

[40] Marshall W 1955 Antiferromagnetism *Proc. R. Soc. London, Ser. A* **232** 48

Lieb E and Mattis D 1962 Ordering energy levels of interacting spin systems *J. Math. Phys.* **3** 749

[41] Liu Z-X, Yang Z-B, Han Y-J, Yi W and Wen X-G 2012 Symmetry-protected topological phases in spin ladders with two-body interactions *Phys. Rev. B* **86** 195122

[42] den Nijs M and Rommelse K 1989 Preroughening transitions in crystal surfaces and valence-bond phases in quantum spin chains *Phys. Rev. B* **40** 4709

White S R 1996 Equivalence of the antiferromagnetic Heisenberg ladder to a single $S = 1$ chain *Phys. Rev. B* **53** 52

Fáth G, Legeza Ö and Sólyom J 2001 String order in spin liquid phases of spin ladders *Phys. Rev. B* **63** 134403

Nakamura M and Todo S 2002 Order parameter to characterize valence-bond-solid states in quantum spin chains *Phys. Rev. Lett.* **89** 077204

Hung H-H, Gong C-D, Chen Y-C and Yang M-F 2006 Search for quantum dimer phases and transitions in a frustrated spin ladder *Phys. Rev. B* **73** 224433

Kim E H, Legeza Ö and Sólyom J 2008 Topological order, dimerization, and spinon deconfinement in frustrated spin ladders *Phys. Rev. B* **77** 205121

[43] Verstraete F, Cirac J I and Murg V 2008 Matrix product states, projected entangled pair states, and variational renormalization group methods for quantum spin systems *Adv. Phys.* **57** 143

Augusiak R, Cucchietti F M and Lewenstein M 2012 Many body physics from a quantum information perspective *Lect. Notes Phys.* **843** 245

Orús R 2014 A practical introduction to tensor networks: matrix product states and projected

entangled pair states *Ann. Phys.* **349** 117

- [44] Jordan J, Orús R, Vidal G, Verstraete F and Cirac J I 2008 Classical simulation of infinite-size quantum lattice systems in two spatial dimensions *Phys. Rev. Lett.* **101** 250602
- [45] Pirvu B, Verstraete F and Vidal G 2011 Exploiting translational invariance in matrix product state simulations of spin chains with periodic boundary conditions *Phys. Rev. B* **83** 125104
- [46] Vidal G, Latorre J I, Rico E and Kitaev A 2003 Entanglement in quantum critical phenomena *Phys. Rev. Lett.* **90** 227902